Reference evapotranspiration from coarse-scale and dynamically downscaled data in complex terrain: sensitivity to interpolation and resolution

Courtenay Strong[a,*], Krishna B. Khatri[b], Adam K. Kochanski[a], Clayton S. Lewis[c], L. Niel Allen[c]

[a]Dept. of Atmospheric Sciences, University of Utah, Salt Lake City, UT 84124, USA

[b]Dept. of Civil and Environmental Engineering, University of Utah, Salt Lake City, UT 84124, USA

[c]Dept. of Civil and Environmental Engineering, Utah State University, Logan, Utah 84321, USA

Summary

The main objective of this study was to investigate whether dynamically downscaled high resolution (4-km) climate data from the Weather Research and Forecasting (WRF) model provide physically meaningful additional information for reference evapotranspiration (E) calculation compared to the recently published GridET framework that uses interpolation from coarser-scale simulations run at 32-km resolution. The analysis focuses on complex terrain of Utah in the western United States for years 1985-2010, and comparisons were made statewide with supplemental analyses specifically for regions with irrigated agriculture. E was calculated using the standardized equation and procedures proposed by the American Society of Civil Engineers from hourly data, and climate inputs from WRF and GridET were debiased relative to the same set of observations. For annual mean values, E from WRF (E_{W}) and E from GridET (E_{G}) both agreed well with E derived from observations (r^2 = 0.95, bias < 2 mm). Domain-wide, E_{W} and E_{G} were well correlated spatially (r^2 = 0.89), however local differences $\Delta E = E_{\mathrm{W}} - E_{\mathrm{G}}$ were as large as +439 mm year^{-1} (+26%) in some locations, and ΔE averaged +36 mm year^{-1}. After linearly removing the effects of contrasts in solar radiation and wind speed, which are characteristically less reliable under downscaling in complex terrain, approximately half the residual variance was accounted for by contrasts in temperature and humidity between GridET and WRF. These contrasts stemmed from GridET interpolating using an assumed lapse rate of Γ=6.5 K km^{-1}, whereas WRF produced a thermodynamically-driven lapse rate closer to 5 K km^{-1} as observed in mountainous terrain. The primary conclusions are that observed lapse rates in complex terrain differ markedly from the commonly assumed Γ=6.5 K km^{-1}, these lapse rates can be realistically resolved via dynamical downscaling, and use of constant Γ produces differences in E of order as large as 10^2 mm year^{-1}.

Key words: Reference evapotranspiration; sensitivity; bias; dynamically downscaled; climatic variables; hydrologic process

---

Corresponding author. Tel.: +1 801-585-0049; fax: +1 801-585-3681.

E-mail address: court.strong@utah.edu (Courtenay Strong).

1 Introduction

Evapotranspiration is one of the key components of the hydrological cycle, and its accurate estimation is important for a variety of applications including regional water and energy budget analyses, water resources management, water demand analysis for agricultural systems, and ecosystem services. Reference evapotranspiration (*E*) refers to the atmospheric evaporative demand for a hypothetical grass reference crop with specific characteristics (Allen et al., 1998; Jensen et al., 1990), and should not be confused with potential evapotranspiration (e.g., McVicar et al., 2012). In estimation of agricultural crop evapotranspiration and crop water requirements, *E* can be multiplied by tabulated coefficients which are specific to a given crop during its initial, mid-season, and end of late season growth stages. However, accurate estimation of evapotranspiration in any location is difficult and challenging due to multiple factors controlling *E* (e.g., air temperature, solar radiation, wind speed, relative humidity), variability and interaction among controlling factors, and often insufficient data (Allen et al., 2011; Estévez et al., 2016; Hobbins, 2016).

Several methods have been developed worldwide to estimate actual evapotranspiration from different climatic variables, and McMahon et al. (2013) provide an excellent review. These methods vary in data requirements from very simple, empirically based or simplified equations requiring only monthly average air temperatures (e.g., Blaney and Criddle, 1962; Hargreaves and Samani, 1985; Jensen and Haise, 1963; Thornthwaite, 1948) to complex, more physically based equations requiring daily or hourly data such as Penman-Monteith method (e.g., Monteith, 1965). Some methods are only valid for specific climatic and agronomic conditions and are not applicable to conditions different from those under which they were originally developed (Allen et al., 1998), although recent research has provided more generalized, physically based methods to estimate potential evapotranspiration (Donohue et al., 2010) and pan evaporation (Roderick et al., 2007).

For crop applications specifically, the American Society of Civil Engineers (ASCE) recommends a Standardized Reference Evapotranspiration Equation (ASCE-ET) to ensure consistency of methods and achieve unity of transferability of crop coefficients from one location to another. The ASCE-ET was derived from the Penman-Monteith equation (ASCE-PM method) by simplifying several terms within that equation and standardizing computational procedures (ASCE-ET) (Allen et al., 2005). The two standardized *E* surface types considered in establishing uniformity in evapotranspiration estimation and transferable crop coefficients are: (1) a short crop with an approximate height of 0.12 m – similar to clipped, cool-season grass, and (2) a tall crop with an approximate height of 0.50 m – similar to full-cover alfalfa. We focus on this formulation here principally because we are interested in direct comparison to the recently developed GridET framework (GridET, 2015; Lewis and Allen, 2016), and we additionally note that this formulation is widely used and offers flexibility with respect to a large suite of specific crops.

Several researchers have analyzed the sensitivity of the ASCE-ET equation to climatic variables in various climatic conditions. Irmak et al. (2006) analyzed sensitivity of the ASCE-ET equation to wind speed, maximum and minimum air temperature, vapor pressure deficit, and solar radiation in the various climatic regions of the United States (i.e., semiarid and semi humid, Mediterranean-type, coastal humid, inland humid, and island). The sensitivity of *E* to climate variables was found to exhibit significant variations between the locations. *E* was in general most sensitive to vapor pressure deficit at all locations, wind speed in semiarid regions, and solar radiation in humid locations. Gavilán et al. (2008) applied the ASCE-ET equation to a region of Spain and found that accuracy of the equation was affected by annual average wind speed and daily temperature range (i.e., difference between daily maximum and minimum air temperature). Estévez et al. (2009) analyzed the sensitivity of *E* to air temperature, relative humidity, solar radiation, and wind speed in semi-arid regions of southern Spain. Their results highlighted significant spatial variability of *E*, and their uncertainty analysis showed that effects from introduced random errors were larger than those of systematic errors.

Recently, Lewis et al. (2014) studied the sensitivity of *E* to climatic parameters at a regional scale over the western United States. They found that hourly wind speeds exhibited the lowest correlation to station observations in the Southern parts of California, Arizona, and much of the Rocky Mountains. Hobbins (2016) analytically derived expression of the sensitivity of daily ASCE-ET to each of the drivers and, contrary to a commonly invoked assumption, found that temperature is not the most significant driver of temporal variability in reference evapotranspiration for all regions and seasons. Summarizing more than 30 studies, McVicar et al. (2012) found that wind speed was commonly in the top two dominant drivers of historical downward trends in atmospheric evaporative demand. Other studies on the sensitivity of *E* to climatic variables is available elsewhere as summarized in Table 1. For example, sensitivity of *E* to changes in humidity, wind speed, and maximum temperature in Spain (Vicente-Serrano et al., 2014); sensitivities of the FAO56 Penman–Monteith equation to climate variables in 668 stations of China from 1960 to 2009 (Zheng and Wang, 2015); sensitivity of evapotranspiration to climatic change in four types of climates (i.e., humid, cold semi-arid, warm semi-arid and arid) in Iran (Tabari and Talaee, 2014); and findings on the spatial and temporal variability of *E* in the Haihe River Basin in present and future stages (Xing et al., 2014).

Despite substantial advances in atmospheric modeling and accessibility of higher resolution meteorological data, the majority of recent studies on *E* analysis are based on coarser scale remote sensing or relatively sparse station-based climate data. Examples include studies based on climatic data derived from satellite remote sensing (e.g., Allen et al., 2007; Kalma et al., 2008, and references therein; Tadesse et al., 2015; Valipour, 2015), data recorded from ground-based weather stations (e.g., Estévez et al., 2016; Irmak et al., 2006; Zheng and Wang, 2015), and climatic data downscaled from coarse resolution regional climate models (Hobbins, 2016).

Many of the studies summarized above found substantial spatiotemporal variability of *E*, and many recommended a comparative study using higher-resolution climate data. Several studies have assessed the value of statistical downscaling for study of atmospheric evaporative demand in complex terrain, often over Asia (e.g., Wang et al., 2013). Although statistical downscaling is computationally efficient, it assumes a spatiotemporal generality of semi-empirical relationships, potentially missing important details resolvable by physically based dynamical downscaling techniques (Gutmann et al., 2012). The value added by dynamical downscaling in complex terrain has been studied for monsoonal and winter precipitation dynamics over Asia (Bhatt et al., 2014; Horvath et al., 2012; Norris et al., 2015) and western North America (Meyer and Jin, 2016; Rasmussen et al., 2011), but comparatively little is known about the value of dynamical downscaling for evaporative demand specifically for agricultural applications. Evaluating the potential of estimating *E* using data downscaled by the Pennsylvania State University – National Center for Atmospheric Research (PSU/NCAR) mesoscale modeling system 5 (MM5; Haagenson et al., 1994), Ishak et al. (2010) found that downscaling generally improved the quality of input variables, except wind speed which exceeded observations by as much as 400%.

The overarching goal of this study was to investigate whether high-resolution dynamically downscaled meteorological data provide physically meaningful additional information for *E* calculation compared to interpolated and coarser-resolution climate data in complex terrain similar to the state of Utah in the western parts of the United States. The study was motivated by the recently published GridET framework which is an open source software package (GridET, 2015) that estimates gridded *E* via the ASCE-ET equation at a user-defined horizontal resolution based on climate inputs from a flexible suite of hourly forcing data sets. We have two specific objectives to support the overarching goal. Objective 1 is to compare *E* results generated by two climactic data sets with differing horizontal resolution, with GridET using climate input variables which are coarser than our dynamically downscaled climate fields. Objective 2 is to determine what fraction of the differences uncovered in Objective 1 are linearly attributable to differences in the input climate fields. In analyzing the sensitivity of the ASCE-ET equation to differences in climate input variables for Objective 2, we are especially interested in effects of lapse rate (change of temperature with altitude) for which GridET assumes a constant value versus a physically resolved value in the dynamical downscaling. These two specific objectives provide the structural sub-headings used in the Methods and Results sections of the manuscript.

2 Data and Methods

2.1 Compare *E* in GridET to higher resolution dynamical downscaling

We used the Weather Research & Forecasting (WRF) model (Skamarock et al., 2005) to dynamically downscale climate drivers of *E* to 4-km horizontal resolution covering Utah for the period from 1985 to 2010. The results were compared with *E* from the GridET software package (GridET, 2015; Lewis and Allen, 2016) which uses climate drivers from the North American Land Data Assimilation System (Mitchell et al., 2004). NLDAS data are provided at 10-14 km horizontal resolution and are derived from the North American Regional Reanalysis simulations performed at 32-km horizontal resolution.

2.1.1 Study Region

Utah features complex terrain representative of much of the western US (Fig. 1) and other arid mountainous regions of the world. Although largely arid, regions of orographic precipitation provide a water supply that supports agriculture. The highest precipitation rates occur in the mountains where streams begin and groundwater recharge occurs. Historically, approximately 90 percent of Utah's fresh water diversions are for irrigation with proportions of about 80 percent (varies annually based on precipitation and water supply) for agriculture irrigation (Maupin et al., 2014) and about 10 percent for urban irrigation (Utah Department of Natural Resources, 2010). Correspondingly, evapotranspiration of irrigated landscapes and crops plays a critical role in water management. Utah's irrigated agriculture area covers 4,590 km^2 or approximately 2.1 percent of the state's area (USDA, 2014). Water diversions in 2005 from surface water and groundwater were 82 percent and 18 percent, respectively (Maupin et al., 2014).

< Figure 1 here please>

2.1.2 Reference evapotranspiration (E) formulation

We used the ASCE-ET equation (Allen et al., 2005) for our calculations, detailing its formulations here for completeness and to establish notation. Derived from the ASCE Penman-Montieth formulation, the equation for hourly reference evapotranspiration can be written

$$\mathrm{E} = \frac{\omega\Psi(\mathrm{R_n} - \mathrm{G}) + \gamma\frac{\mathrm{C_n}}{\mathrm{T} + 273}\mathrm{V}(\mathrm{e_s} - \mathrm{e_a})}{\Psi + \gamma(1 + \mathrm{C_d}\mathrm{V})}, \tag{1}$$

where $\omega = 0.408\ \mathrm{m^2\ mm\ MJ^{-1}}$, R_n is net radiation (MJ $\mathrm{m^{-2}\ h^{-1}}$), G is soil heat flux density at the soil surface (MJ $\mathrm{m^{-2}\ h^{-1}}$), $\gamma = 6.65{\times}10^{-3}p$ is the psychrometric constant (kPa $\mathrm{K^{-1}}$) for station pressure p (kPa), e_s is saturation vapor pressure (kPa), e_a is actual vapor pressure (kPa), $\Psi = \partial e_\mathrm{s}/\partial T$ (kPa $\mathrm{K^{-1}}$), and the following parameters were used to correspond to hourly calculation for a tall reference crop such as alfalfa: $\mathrm{C_n} = 66\mathrm{K\ mm\ s^3\ h^{-1}}$, $\mathrm{C_d} = 0.25\ \mathrm{s\ m^{-1}}$ for daytime, and $\mathrm{C_d} = 1.7\ \mathrm{s\ m^{-1}}$ for nighttime. In our application, four meteorological variables were used to derive the input quantities (e.g., $\mathrm{R_n}$) required for the ASCE-ET formula: 2-meter air temperature (T), 2-meter relative humidity (RH) or specific humidity (q), 2-meter wind speed (V), and downward solar radiation at the surface (S). For consistency with GridET, the formulas used to derive the input quantities from these four meteorological variables follow (Allen et al., 2005).

Several studies indicate that the ASCE-ET equation may overestimate *E* under conditions where wind speeds are large or highly variable (Hill et al., 2011). For consistency with GridET, hourly V in the WRF output was limited to 2.5 m s^{-1} following (Lewis and Allen, 2016). As detailed by Lewis and Allen (2016), the rationale for capping the wind speed was based on prior observational analyses using the ASCE-ET equation in this study region.

2.1.3 Grid ET

GridET is an open source software package (GridET, 2015) that estimates gridded *E* by the ASCE-ET and other equations at a user-defined horizontal resolution based on meteorological inputs from hourly NLDAS (Mitchell et al., 2004) forcing data set (T, *q*, surface air pressure, 10-meter wind speed, and bias-corrected S). In addition, GridET calculates daily potential evapotranspiration by the crop coefficient method (Allen et al., 1998) and determines net potential evapotranspiration by subtracting interpolated effective precipitation from the 1-km DAYMET data set (Thornton et al., 2012). A lapse rate of $\Gamma = -\partial \mathrm{T}/\partial \mathrm{z} = 6.5 \ \mathrm{K\,km^{-1}}$ was used to produce near surface elevation dependence (NSED,McVicar et al., 2007) in T and hence e_s. Constant Γ was used for consistency with (Lewis and Allen, 2016) and the GridET framework (GridET, 2015), and the underlying rationale was to replicate NLDAS procedures in downscaling from the North American Regional Reanalysis (Cosgrove et al., 2003; Mesinger et al., 2006). RH was computed from NLDAS T, *q*, and *p* and then bilinearly interpolated to determine e_a. NLDAS V fields were also bilinearly interpolated, resolved to a magnitude, and limited to 2.5 m s^{-1} as noted in Section 2.1.2. For S, NLDAS downward solar radiation was adjusted for aspect and slope following (Allen et al., 2006). Lewis and Allen (2016) provide further details and observational validation of GridET, including development of the *E* input variables on a 0.54-km resolution grid covering the state of Utah following methodology validated against 704 agriculturally-situated weather stations (Lewis et al., 2014).

2.1.4 Regional climate simulation using WRF

We used the Weather Research & Forecasting (WRF) model (Skamarock et al., 2005) to dynamically downscale climate drivers of E to a 4-km horizontal resolution domain covering Utah for years 1985-2010. Initial and lateral boundary conditions were derived from 6-hourly Climate Forecast System Reanalysis (CFSR; Saha et al., 2010) data at 38-km horizontal resolution. We used a nested domain configuration with an outer 36-km resolution domain (d01) receiving lateral boundary conditions from CFSR, with a 12-km resolution nested domain (d02) covering the western US, and an innermost 4-km domain (d03) covering Utah (Fig. 1). The framework included a thermodynamic slab model of the Great Salt Lake with salinity adjustments to saturation vapor pressure over the lake (Strong et al., 2014). Additional configuration details and historical validation can be found in (Scalzitti et al., 2016). Although some of the input fields for E were available directly in the WRF output (e.g., net radiation), we used only T, V, p, S, and RH based on the water vapor mixing ratio from WRF, and derived the remaining variables as outlined in the ASCE-ET equation. This provided consistency with GridET and allowed more direct comparison to observationally-based calculations of E. Also for consistency with GridET, the horizontal wind speeds from WRF were capped at 2.5 m s^{-1} to avoid a systematic positive bias of WRF relative to GridET which would confound discovery and analysis of temperature and humidity effects.

2.1.5 Debiasing

For GridET, NLDAS climate fields were debiased relative to agriculturally-situated Electronic Weather Station (EWS) data following procedures in (Lewis and Allen, 2016; Lewis et al., 2014). In these prior studies, EWS datasets were selected by fitness of location in representing *E* calculations from 7 different networks in the study area totaling 48 locations. Emphasis was given to deletion of any suspect records over correction with an annual time span being required for inclusion resulting in variable histories from 1986-2010 at each EWS location (8671 total years). An analogous debiasing was performed on the WRF data here. Specifically, WRF *T* and RH were bilinearly interpolated to the locations of the EWS data (gray circles, Fig. 2a), and hourly biases $b_{\mathrm{t,h,i}}$ were calculated for each variable, where $0 \le t \le 364$ is day of year, $0 \le h < 24$ is hour, and $\mathrm{i} \in \{1,2,\ldots,33\}$ is a station index. A statistical model of the bias was written

$$\mathrm{b_t} = \alpha_0 + \alpha_1 \cos\left(\frac{2\pi \mathrm{t}}{364} - \phi_1\right) + \alpha_2 \cos\left(\frac{2\pi \mathrm{h}}{24} - \phi_2\right) + \alpha_3 \mathrm{g_{t,h}} + \epsilon_{\mathrm{t}}, \qquad (2)$$

where $\mathrm{g_{t,h}}$ is the value of the variable being debiased, ϵ_{t} is a residual term, and the coefficients $\alpha_{\mathrm{j}}, \mathrm{j} = 1,2,3$ were calculated to minimize the domain-wide sum of squared residuals. Note that (2) varies in time but not space as in (Lewis and Allen, 2016).

< Figure 2 here please >

2.1.6 Comparison of WRF and GridET

GridET and WRF data are shown in their native resolutions when mapped. Where comparisons between GridET and WRF were made, the 0.54-km GridET data were coarsened to the 4-km WRF grid by spatial averaging. To accomplish the averaging, for each of the 863,214 points in the GridET data, we determined the index of the closest point on the WRF grid. The overlapping spatial domain had 1,301 grid points where fluxes associated with WRF's specialized treatment of fluxes over lakes, urban areas, and barren regions such as the Bonneville Salt Flats (Fig. 2c) generated climate inputs with expectedly large differences from NLDAS fields. These grid points, amounting to 4% of WRF's d03 domain had minimal overlap with irrigated agriculture (compare Fig. 2b,c), and results are sometimes mapped at these locations and always excluded from statistical analyses. Also, the excluded lake regions were dilated one pixel in each direction to account for modification of near-surface temperature and humidity by lake effects (e.g., due to diurnal lake breezes).

2.2 *Analysis of linear effects*

2.2.1 Linear statistical model

We use E_G to denote the spatial vector of long-term mean E from GridET, and E_W to denote the spatial vector of long-term mean E from WRF dynamical downscaling (these vectors have 1,301 components, each corresponding to one location of the overlapping grid). The variance in $\Delta E = E_W - E_G$ was analyzed using the linear statistical model

$$\Delta E = \beta_1 \Delta V + \beta_2 \Delta S + \beta_3 \Delta T + \beta_4 \Delta T_d + \epsilon, \qquad (3)$$

where the β terms are multiple linear regression coefficients and ϵ denotes residuals. Use of a linear model is supported by nonlinearity being mild in the ASCE-ET equation (Hobbins, 2016). Insight into ΔE is available by linearly removing the effects of one or two climate inputs at a time. We first remove the effects of ΔS and ΔV to isolate and focus analysis on the effects of differences in humidity and temperature. Our rationale is that ΔS and ΔV represent weaker impacts for most of the study region (Hobbins, 2016), especially considering the wind speed cap noted above. Moreover, we have relatively low confidence in the physical meaningfulness of ΔS and ΔV given several studies concluding that dynamical downscaling in complex terrain does not necessarily improve observational validation of wind speed (e.g., Cheng and Steenburgh, 2005; Jiménez and Dudhia, 2012; Shimada et al., 2011) or solar radiation (e.g., Ruiz-Arias et al., 2016). Temperature and humidity, although subject to bias, often have more favorable outcomes from downscaling in complex terrain (e.g., Heikkilä et al., 2011).

2.2.2 Lapse rate effects

To establish observational lapse rates for comparison to WRF and GridET, we used National Oceanic and Atmospheric Administration (NOAA) monthly climate normals corresponding to 1981-2010 (Arguez et al., 2012), and compared them to normal from our 1985-2010 simulation period. Stations used in the analysis spanned elevations from 1,310 to 2,664 m to capture changes from near valley floor up into the Wasatch Range.

3 Results

3.1 Comparison between *E* from GridET and E from dynamical downscaling

3.1.1 Debiasing results

Averaged across EWS stations for all available observation times (~40,000 observations at each of 33 stations), WRF prior to debiasing had a 0.5°C warm bias, and a dry bias of -5.6% in relative humidity. Although a thorough investigation of the sources of these biases is beyond the scope of this study, our results seem to confirm some of the findings of Coniglio et al. (2013). Their analysis showed that the Mellor-Yamada-Janjić planetary boundary layer scheme (Janjić, 2002) utilized in our downscaling configuration tends to underestimate vertical mixing and overestimate surface temperatures. Relative humidity is temperature dependent (i.e., decreases as the temperature increases for a constant mass of moisture in the air), so too high surface temperature leads to too low relative humidity, which may partially explain the dry model bias. The biases may also be attributed to cooling and increased humidity from irrigated crop evapotranspiration, which is not explicitly treated in WRF. For solar radiation, WRF had a tendency to overestimate S, possibly because of its deficiency in accurate representation of the cloud coverage and the radiative effects of cumulus clouds (Ruiz-Arias et al., 2016). Also, the absence of cumulus parameterization in our convection-permitting 4-km d03 domain could result in an underestimation of solar shading by convective clouds which are too small to be resolved on the model grid. In order to compensate for these deficiencies, the WRF simulated S was debiased based on NLDAS data which were bias-corrected relative to observations (Berg et al., 2003), meaning a monthly mean domain-wide bias (WRF minus NLDAS) averaging 40 W m^{-2} was subtracted from the S values produced by WRF. Not removing this difference in S would have yielded E values approximately 10% larger in WRF compared to GridET. As noted in Section 2.1.3, we capped the wind speeds at 2.5 m s^{-1} for consistency with GridET. Domain-wide for the analysis period, 61% of the hourly wind speed observations required application of the cap. The percentage of hourly wind speed observations that were capped exhibited a strong elevational dependence, with the highest local capping percentages occurring at the highest elevations, as we would expect from wind speed climatology in complex terrain. Without the wind speed cap, long-term mean E from WRF would have increased by an average of 12% on the overlapping analysis domain.

3.1.2 Agreement with observationally-derived E

Here, we examine how *E* from WRF (E_W) and *E* from GridET (E_G) compare with values of *E* derived from the electronic weather stations whose locations are indicated in Fig. 2a. We would expect good agreement because the inputs to E_W and E_G were debiased relative to data from these stations. The purpose of presenting this comparison is thus to verify the efficacy of the debiasing procedure, not to pose or fit a statistical model. As shown in Fig. 3, monthly ET from each framework yielded values correlated with station-based E at $r^2 = 0.95$, and each had a small bias (-0.3 mm for GridET and 1.1 mm for WRF). Ensuring that the two frameworks have similar agreement with station-based values after identical debiasing procedure enables us to meaningfully investigate how the frameworks differ away from the debiasing stations.

< Figure 3 here please>

3.1.3 Annual mean comparison

Mean annual *E* generally increased toward southern portions of the state where temperatures and solar radiation were higher, but was strongly influenced by Utah's complex terrain in both GridET and WRF, with a tendency for higher values at lower elevations (Fig. 4a,b; elevation shown in Fig. 2a). The larger magnitude differences in the map of $\Delta E = E_W - E_G$ were predominantly positive except toward the northern portion of the analysis domain (Fig. 4c). Long-term mean values of *E* at each grid point were well correlated spatially between WRF and GridET (r^2=0.89, Fig. 5a). E_W tended to be larger for large values of *E* and smaller for small values of *E* (compare data and one-to-one line, Fig. 5a), and the spatial average of the long-term mean *E* (i.e., the mean of the data in Fig. 5a) was 36 mm year^{-1} (2%) larger in WRF than in GridET

[1,509 mm year^{-1} versus 1,473 mm; root mean square deviation (RMSD) was 89 mm year^{-1}]. The spatial average of the temporal variance of *E* (i.e., the variance of the data in Fig. 5a) was 1.6 times larger in WRF than in GridET (51,224 mm^2 year^{-2} versus 32,605 mm^2 year^{-2}). Restricting to grid points with irrigated agriculture (dark gray data, Fig. 5a), and to seasons (Fig. 5d) did not change these overall tendencies.

< Figure 4 here please >

< Figure 5 here please >

3.2 Linear effects

3.2.1 Comparison of climate input variables

We now consider differences in the climate input variables obtained from WRF and GridET, noting that approximately half of the variance in ΔE can be linearly modeled by these differences (shown below in Section 3.3). Annual mean T in WRF (T_W) was highly spatially correlated ($r^2 = 0.94$; $RMSD = 1.2$°C) with annual mean T in GridET (T_G) (Fig. 4d,e and Fig. 5b). The difference $\Delta T = T_W - T_G$ had an elevational dependence, with a tendency for positive values in higher terrain and negative values in lower terrain (compare Fig. 4f to Fig. 2a). The associated scatterplot indicated that positive ΔT was equivalently associated with locations that were overall cooler (and negative ΔT with locations that were overall warmer) (Fig. 5b), and this tendency persisted when restricting to grid points with irrigated agriculture (compare data and one-to-one line, Fig. 5b), and also when restricting to seasons (Fig. 5e). For annual data, WRF had a higher mean temperature (8.0°C versus 7.5°C) and a smaller variance (7.3°C^2

versus 12.0°C^2). These ΔT results stemmed largely from the lapse rate used for interpolation in GridET being larger than the lapse rate resolved by WRF as shown below in Section 3.4.

The overall spatial correlation of dew point temperature in WRF ($T_{d,W}$) and in GridET ($T_{d,G}$) was high ($r^2 = 0.92$ with RMSD=1.5°C, Fig. 4g,h; Fig. 5c). The strongest contrasts in T_d were predominantly positive when mapped as $\Delta T_d = T_{d,W} - T_{d,G}$, indicating a tendency for higher dewpoints in WRF, especially at higher elevations (Fig. 4i). This tendency persisted when restricting to grid points with irrigated agriculture (compare dark gray points and one-to-one line, Fig. 5c), and also when restricting to seasons (Fig. 5f). These contrasts stemmed from the stronger GridET lapse rate noted above projecting onto the recovery of T_d from RH. To illustrate this projection, the approximate formula (Lawrence, 2005) T_d = T - (100-RH)/5 shows that a larger lapse rate yielding a lower temperature at high elevations in GridET would produce a lower dewpoint for the same RH. For annual data over the study domain, WRF had a higher overall T_d (-1.2°C versus -2.3°C), and the variance in WRF was substantially smaller (2.3°C^2 versus 5.7°C^2).

The spatial correlation between annual mean 2-meter wind speed in WRF (V_W) and in GridET (V_G) was small ($r^2 = 0.20$), in part because V_G was bilinearly interpolated from NLDAS data which were based on 32-km horizontal NARR output (Fig. 4j), whereas V_W was simulated on terrain resolved at 4-km horizontal resolution (Fig. 4k). ΔV was predominantly positive (Fig. 4l), but averaged only 0.22 m s^{-1} in magnitude in part because of the imposed wind speed cap noted in Section 2.

Annual mean S in WRF (S_W) was moderately correlated ($r^2 = 0.58$) with annual mean S in GridET (S_G). Both S_G and S_W were pre-albedo values, so surface reflectivity (e.g., from snow cover) exerted no direct effect on ΔS. S_G and S_W both accounted for terrain effects by calculating solar incidence angle based on slope and aspect (e.g., Garnier and Ohmura, 1968), but some details of the GridET algorithms (Allen et al., 2006) differed from the radiation scheme used in WRF (Barlage et al., 2010), potentially generating terrain-dependent effects (Fig. 4m,n). Finally, there appeared to be a rectangular artifact in S_G in the northwestern portion of the state (Fig. 4m) that resulted in large positive ΔS over the same region (Fig. 4o).

3.2.2 Statistical model of linear effects

More than two-thirds of the variance in $\Delta \mathrm{E}$ was accounted for by the linear statistical model given by (3) as shown in Fig. 6a. ΔV and ΔS each accounted for approximately 20% of the variance in ΔE (Fig. 6b,c), and the linear model combining their effects

$$\Delta E = \gamma_1 \Delta V + \gamma_2 \Delta S + \epsilon, \qquad (4)$$

accounted for 33% of the variance in ΔE (Fig. 6d). We use the notation ΔE^* to denote ΔE with the effects of ΔV and ΔS linearly removed [i.e., the residuals from the model given by equation (4)], and ΔE^* is shown in map view in Fig. 7a. Removing the linear effects of $\Delta \mathrm{V}$ and ΔS exposed the dependence of $\Delta \mathrm{E}$ on elevation (Fig. 7; Fig. 8a). Some of this elevational dependence of $\Delta \mathrm{E}^*$ was due to the above-noted tendency for WRF to have higher dew points than GridET at higher elevations (and thus lower E; Fig. 8b). ΔE^* was negatively correlated with ΔT_d (Fig. 8b) with no significant relationship to ΔT (Fig. 8c). However, ΔT explained residual variance in ΔE^* after linearly removing the effect of ΔT_d, and the model

$$\Delta E^{*} = \gamma_1 \Delta T_d + \gamma_2 \Delta T + \epsilon \tag{5}$$

accounted for slightly more than half of the ΔE^{*} variance (Fig. 8d). Standardizing the predictors to facilitate comparison of the regression coefficients yields values ($\gamma_1 = -97.3$; $\gamma_2 = 70.7$) consistent with physical reasoning. Specifically, higher dew points in WRF tended to yield negative ΔE^{*} by reducing E_{W}, whereas higher temperature in WRF tended to yield positive ΔE^{*} by increasing E_{W}.

< Figure 7 here please >

< Figure 8 here please >

3.2.3 Lapse rate effects

The ΔT and ΔT_d patterns highlighted above are dependent on elevation, with WRF being warmer and moister than GridET above approximately 1,500 m and cooler and drier than GridET below (Figure 9a,b). These contrasts are consistent with GridET interpolating with a lapse rate ($\Gamma = 6.5$ K km^{-1}) which is larger than the lapse rate generated by WRF and also larger than the lapse rates found from observational studies of monthly mean temperatures in complex terrain [e.g., 3.9-5.2 K km^{-1} (Minder et al., 2010)]. As context for these results, note that WRF resolves a dynamic humidity profile based on water mass conservation, whereas GridET determines T_{d} via spatial interpolation of relative humidity and an assumed constant Γ.

< Figure 9 here please >

As noted in Section 2.2.2, we established observational lapse rates for comparison to WRF and GridET using NOAA monthly climate normals corresponding to 1981-2010 (Arguez et al., 2012), and compared them to normal from our 1985-2010 simulation period. Stations used in the analysis (filled circles on map in Fig. 10) spanned elevations from 1,310 to 2,664 m. For locations labeled northwest on the map in Fig. 10, and considering fall (September-October) as an example, the observationally-based lapse rate was $\Gamma_\mathrm{O} = 5.8 \pm 1.5$ K km^{-1} (blue circles with black regression line, Figure 9c). The WRF grid points within the latitude-longitude range of these observation stations had a similar lapse rate of $\Gamma_\mathrm{W} = 5.5 \pm 0.1$ K km^{-1}, whereas the GridET lapse rate $\Gamma_\mathrm{G} = 7.0 \pm 0.1$ K km^{-1} was notably larger (Figure 9c). Similar results were obtained using the west central locations, although few degrees of freedom inflate the confidence bounds on the observed values (Figure 9d). Repeating this analysis for each month of the year for five clusters of stations, we find overall closer agreement between WRF and observations, each featuring a larger-amplitude annual cycle of lapse rates compared to GridET (curves, Fig. 10) as well as a smaller annual mean lapse rate (horizontal lines, Fig. 10).

< Figure 10 here please >

4 Discussion

We compared and mapped the results of reference evapotranspiration (E) calculation covering the state of Utah from year 1985 to 2010 based on the ASCE-ET equation and two sources of climatic variables: those downscaled from the WRF model in a 4-km horizontal resolution and those provided in the NLDAS model at ~14-km resolution (derived from NARR simulations at 32-km). For annual mean values, E from WRF (E_W) and E from GridET (E_G) both agreed well with E derived from observations ($r^2 = 0.95$, bias < 2 mm). Domain-wide, E_W and E_G were well correlated spatially ($r^2 = 0.89$), however local differences $\Delta E = E_W - E_G$ were as large as

+439 mm (+26%) in some locations, and ΔE spatially averaged +36 mm (+2%). Annual total E_W was larger than E_G at higher values of E, and had had 1.6 times the variance. Linearly removing the effects of contrasts in solar radiation and wind speed, which are characteristically less reliable under downscaling in complex terrain, approximately half of the residual variance was accounted for by contrasts in temperature and humidity between GridET and WRF. GridET interpolated using an assumed lapse rate of 6.5 K km^{-1}, whereas WRF produced a topographically-responsive lapse rate closer to 5 K km^{-1} as observed in mountainous terrain. WRF also resolved topographically-responsive vertical variations in humidity, whereas GridET bilinearly interpolated RH from NLDAS to determine vapor pressure.

Values of E would optimally be based on observed inputs alone, but this is generally not feasible due to the scarcity of suitable station data. Some method of infilling between observations is necessary drawing on interpolation techniques, remotely sensed data, or regional modeling, and associated biases must be accounted for in all methods. GridET was shown in prior work to compare well with station-based reference ET after debiasing. Here, applying analogous debiasing to WRF, we found reasonable overall agreement with GridET, but with some large local contrasts. GridET's ability to resolve effects in complex terrain is ultimately limited by the native 32 km resolution of the NARR data that inform NLDAS, and GridET downscales to higher-resolution temperature and hence humidity fields by using an assumed lapse rate in conjunction with high-resolution terrain maps. Likewise, it achieves higher-resolution solar fields by combining solar angle formulations with high-resolution slope and aspect data. Overall, these terrain-based methods for downscaling the NLDAS fields yield values for E that correlate well spatially with the values based on dynamically downscaled 4-km

WRF fields, although there were large local differences in magnitude where substantial vertical interpolation away from observation stations was necessary.

Prior research summarized in Table 1 strongly emphasizes the importance of quality meteorological inputs for reliable estimates of *E*, and highlights potential pitfalls such as inadequate sampling in space or time (Estévez et al., 2016; Hupet and Vanclooster, 2001). Based on comparison of downscaling to interpolation assumptions, the present study indicates that lack of spatial sampling of temperature in complex terrain can yield errors in *E* order 10^2 mm $year^{-1}$. Although atmospheric evaporative demand is highly responsive to spatial and temporal variations in temperature (e.g., Vicente-Serrano et al., 2014; Xing et al., 2014), many studies emphasize regionally strong dependencies on humidity and solar radiation (Irmak et al., 2005; Tabari and Talaee, 2014; Zheng and Wang, 2015), and downward global trends in evaporative demand have been conclusively linked to wind speed trends (McVicar et al., 2012). Our results support the finding that downscaling methods can improve the quality of meteorological inputs (Ishak et al., 2010), but detailed attention is needed to associated biases which can be quite large for variables that depend on parameterization schemes (e.g., solar radiation depends on semi-empirical cloud fraction algorithms).

Reliable calculations of E are essential for decision making by state water managers, and there is substantial interest in extending E calculations into the future to assess how climate change and population growth will affect water availability (USBR, 2012). Additionally, many existing river compacts (e.g. Bear River and Colorado River) rely upon estimated consumptive use for water administration and allocation (Utah Code, 2016). This temporal extension introduces two additional challenges. First, without observational guidance, future calculations depend entirely on model output, underscoring the importance of assessing and observationally validating various downscaling techniques within the historical record. Second, models in general exhibit a bias under historical validation, and use of a model in the future requires a debiasing scheme that typically assumes the historical bias appears unchanged in the future simulation which may not be true (this applies to the regional model itself and lateral boundary conditions drawn from one or more global climate models).

5 Conclusion

We conclude that the terrain-responsive dynamical downscaling provided by WRF provides meaningful temperature and humidity information beyond lapse rate-based interpolation of coarser scale fields as applied in GridET. Observed lapse rates in complex terrain differ markedly in space and time from the commonly assumed Γ=6.5 K km^{-1}, these lapse rates can be realistically resolved via dynamical downscaling, and use of constant Γ produces differences in E of order 10^2 mm year^{-1}. Nonetheless, the computational expense of WRF is substantial, and the ability to achieve comparable results with readily available, coarser-scale NLDAS fields makes the GridET methodology attractive, especially if results are restricted to elevations where observations are available to inform debiasing. Considering the strong dependence of E on temperature, if lower resolution data are to be used for estimation of E, dynamical or observational methods should be used to account for local and seasonal variations in lapse rate. This is especially valid in cases where agriculture resides at elevations that require substantial vertical extrapolation away from observation sites or coarse-scale model grid points.

Regional climate simulation at high resolution or at coarse scale with interpolation from appropriate lapse rates provide suitable methods for extension of reference ET analyses into the future, and this is work the authors currently have underway.

Acknowledgments

The authors thank the Editor, Associate Editor, and three anonymous reviewers for comments that helped to improve the manuscript. Computing resources (ark:/85065/d7wd3xhc) were provided by the Climate Simulation Laboratory at NCAR's Computational and Information Systems Laboratory, sponsored by the National Science Foundation and other agencies. Provision of additional computer infrastructure by the Center for High Performance Computing at the University of Utah is gratefully acknowledged. This material is partially based upon work supported by the National Science Foundation under grants EPS-1135482, EPS-1135483, and EPS-1208732

Table 1. Summary of findings on reference evapotranspiration with attention to complex terrain effects and sensitivity to inputs variables. *T* is air temperature, *V* is wind speed, *RH* represents relative humidity or dew point, and *S* is solar radiation.

Study	Input data	Input resolution	Key findings
1. Allen et al. (1998)	station data	observation network	An improved ASCE-ET formulation for *E* can be scaled to represent variable crop conditions
2. Hupet and Vanclooster (2001)	station data	customized field site	*S* and *V* are the most sensitive to bias stemming from inadequate temporal sampling frequency
3. Irmak et al. (2005)	station data	observation network	*E* was most sensitive to vapor pressure deficit across a range of climate regions in the US
4. Ishak et al. (2010)	MM5 regional climate model	1-km	downscaling generally improved the quality of input variables, except wind speed which exceeded observations by as much as 400%
5. McVicar et al. (2012)	station data from multiple studies	observation network	*V* was commonly in the top two dominant drivers of reported downward trends in atmospheric evaporative demand
6. Vicente-Serrano et al. (2014)	station data	observation network	observed drought in southern Europe stemmed from *T*-driven increases in evaporative demand
7. Tabari and Talaee (2014)	station data	observation network	sensitivity to *V* and *T* in Iran decreased from arid to humid climate, whereas sensitivity to *S* increased
8. Zheng and Wang (2015)	station data	observation network	*S* most important driver overall for China, but *T* and *RH locally* more important toward the north
9. Hobbins (2016)	NLDAS-2	NARR 32-km data interpolated to	T is neither always nor everywhere the most

		0.125° (13.9-km) for NLDAS-2	significant driver of temporal variability over the continental US
10. Xing et al. (2014)	historical station data; future global climate model (GCM) data	historical observation network; GCM ~3° (334-km) data interpolated to 1° (111-km)	Increasing trend during 21st century over Haihe River Basin mainly attributable to projected increases in *T*
11. Estévez et al. (2016)	Station data	Observation network	Relative scarcity of *S* data crucially impacts reliability of *E* calculation in Argentina
12. Lewis and Allen (2016)	NLDAS-2	NARR 32-km data interpolated to 0.125° (13.9-km) for NLDAS-2	Interpolation from NLDAS yielded favorable agreement with estimates based on agriculturally-situated observations
13. This study	WRF regional climate model compared to NLDAS-2	4-km (WRF)	Assumed lapse rates used for interpolation of inputs over complex terrain alter *E* by up to 26% on annual mean basis compared to dynamical downscaling

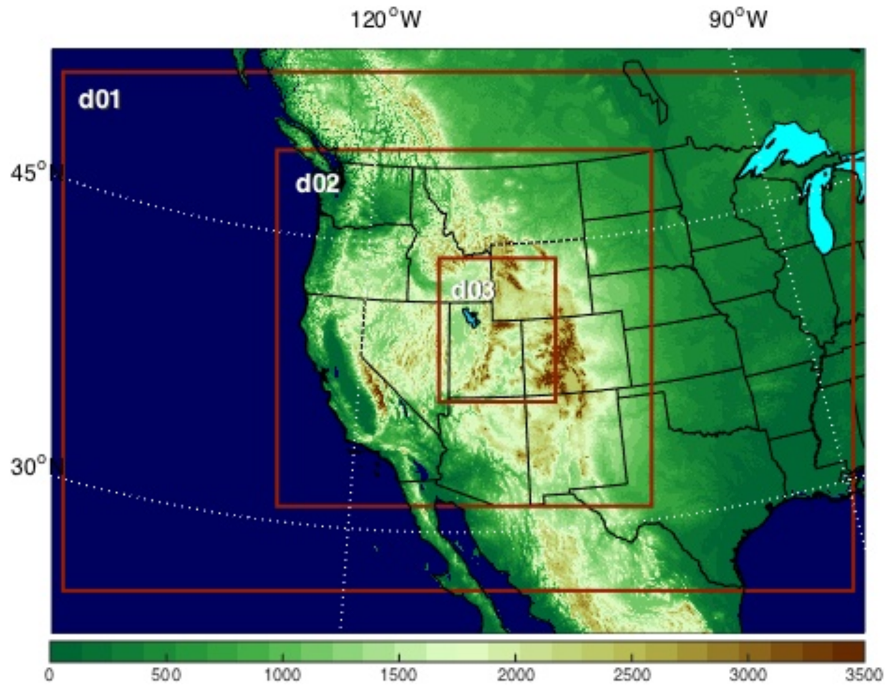

Fig. 1. Simulation domain for the WRF climate model. Rectangles indicate the nested structure with 36-km resolution on domain d01, 12-km resolution on domain d02, and 4-km resolution on the d03 encompassing Utah State. Shading indicates elevation in meters.

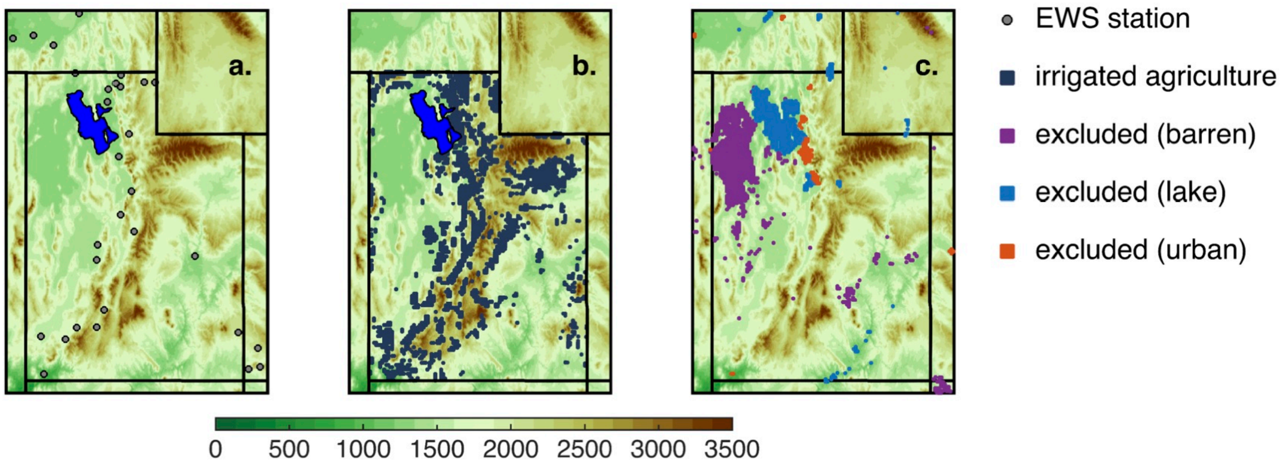

Fig. 2. Observation station locations and surface properties. (a) The d03 domain from Fig. 1a with gray circles indicating locations of Electronic Weather Station (EWS) sites used in debiasing. Shading indicates elevation in meters with the Great Salt Lake shaded blue. (b) Indigo shading indicates WRF grid boxes that contain irrigated agriculture. (c) WRF grid boxes that are excluded from analysis because their WRF land use classification yielded anticipatable large differences from NLDAS (purple indicates barren land such as the salt flats west of the Great Salt Lake, blue indicates lake, and orange indicates urban).

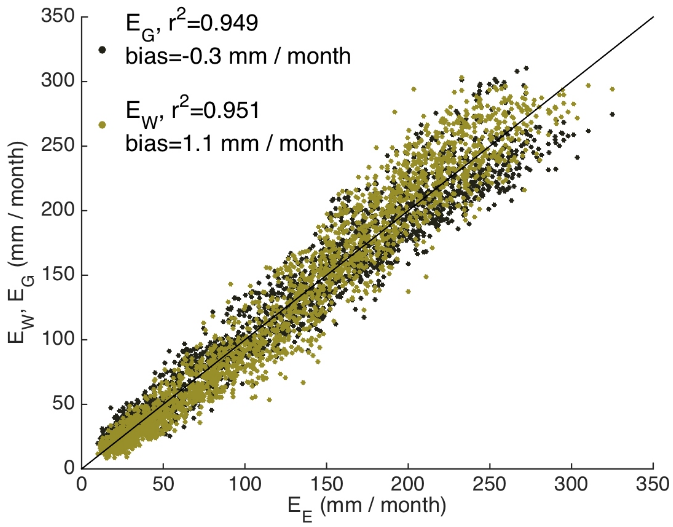

Fig. **3**. Comparison to values derived from observation station data. The abscissa is monthly reference evapotranspiration based on climate inputs observed at Electronic Weather Stations (E_E). The ordinate is monthly reference evapotranspiration based on GridET (E_G) and based on WRF (E_W).

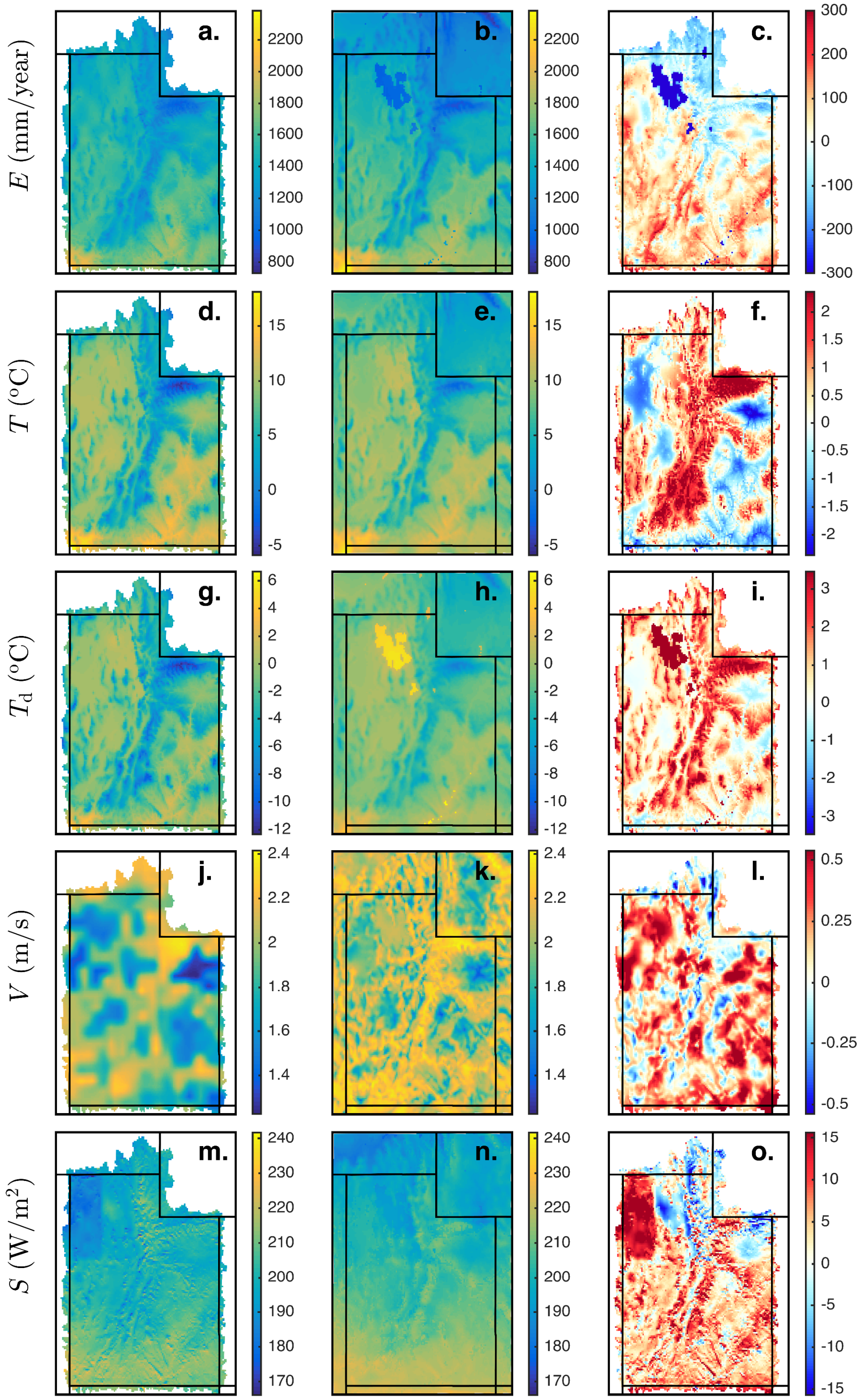

Fig. 4. Maps of annual mean *E* and its input variables. Averaged over years 1985-2010, (a) annual total reference evapotranspiration (E) from GridET), (b) E from WRF, and (c) E from WRF minus E from GridET. Subsequent rows are same as (a-c), but for (d-f) mean 2-m air

temperature T, (g-i) mean 2-m dew point temperature T_d, (j-l) mean 2-m wind speed V, and (m-o) downward solar radiation at surface S.

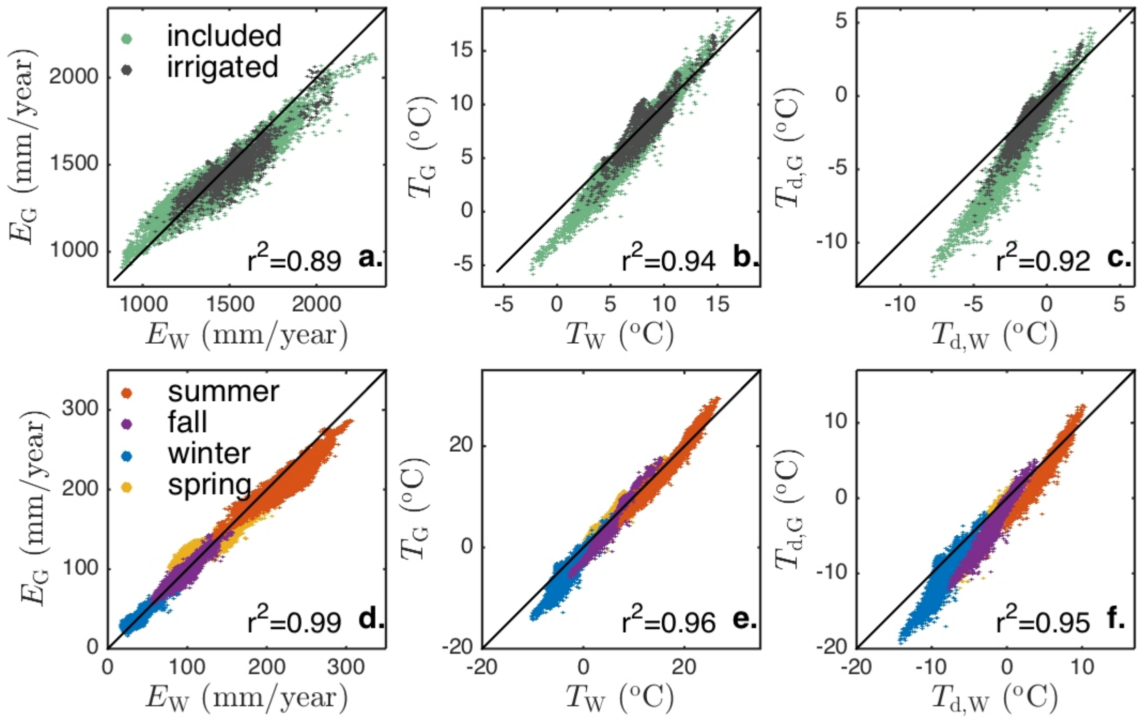

Fig. 5. Scatter plots of annual mean E and its input variables. (a) Annual reference evapotranspiration from GridET (E_G) versus reference evapotranspiration from WRF (E_W). Green symbols correspond to included grid points (i.e., locations not indicated as excluded in Fig. 2c), and gray symbols correspond to grid points that contain irrigated agriculture as indicated in Fig. 2b. Gray line is one-to-one. (b,c) Same as (a), but comparing 2-m air temperature and 2-m dew point temperature, respectively. (d-f) Same as (a-c), but monthly means are restricted to particular seasons as indicated by shading (summer is June-August, fall is September-November, winter is December through February, and spring is March-May).

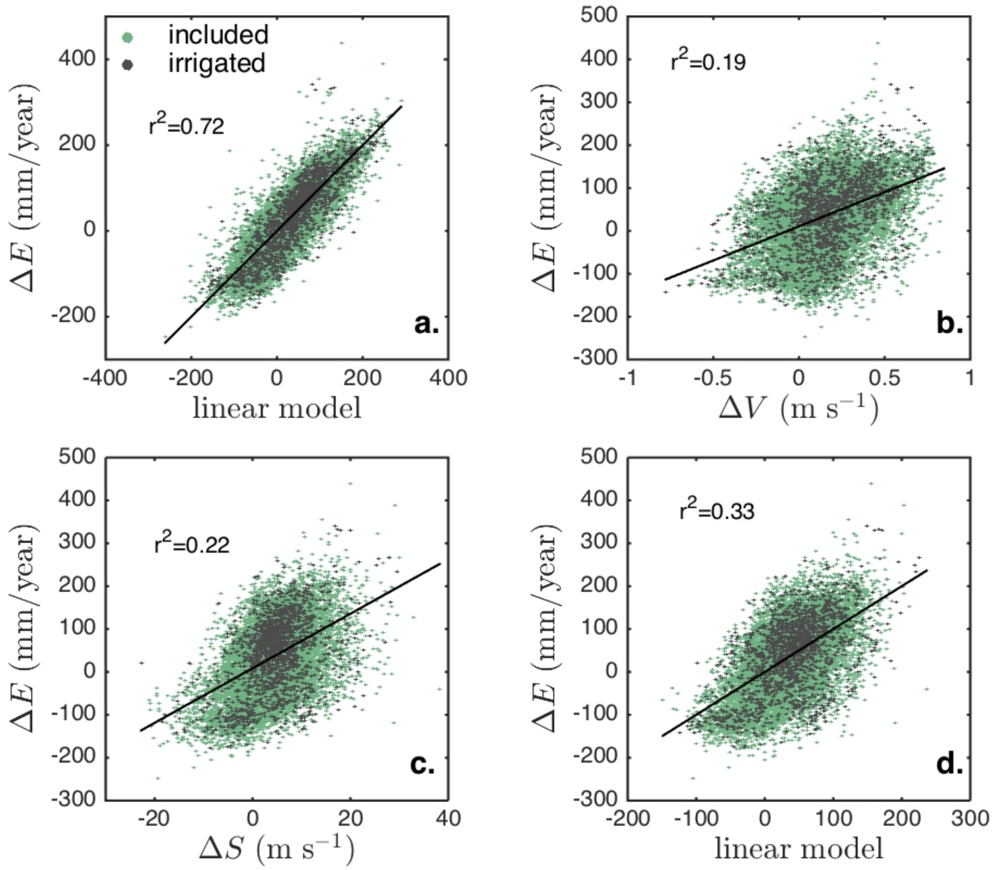

Fig. 6. Linear dependencies of differences in *E*. On the ordinate of each panel, ΔE is average annual data from Fig. 4c. The abscissas are (a) the linear model given by equation (3), (b) ΔV from Fig. 4l, (c) Δ*S* from Fig. 4o, and (d) the linear model given by equation (4). Green symbols correspond to included grid points (i.e., locations not indicated as excluded in Fig. 2c), and gray symbols correspond to grid points that contain irrigated agriculture as indicated in Fig. 2b. Black lines indicate least squares linear regressions.

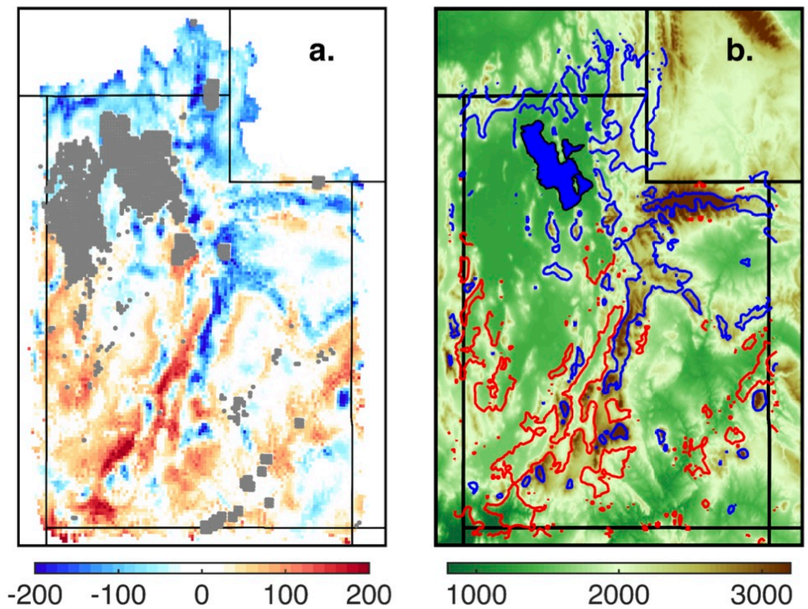

Fig. 7. Differences in E with wind and solar effects removed. (a) Map of ΔE^* which is ΔE with the effects of ΔV and ΔS linearly removed [i.e., the residuals from equation (4)]. Gray shading indicates regions excluded because of their surface types according to Fig. 2c. (b) Contours show two levels sets of ΔE^*: +75 mm (red) and -75 mm (blue) from panel (a). Shading indicates elevation in meters.

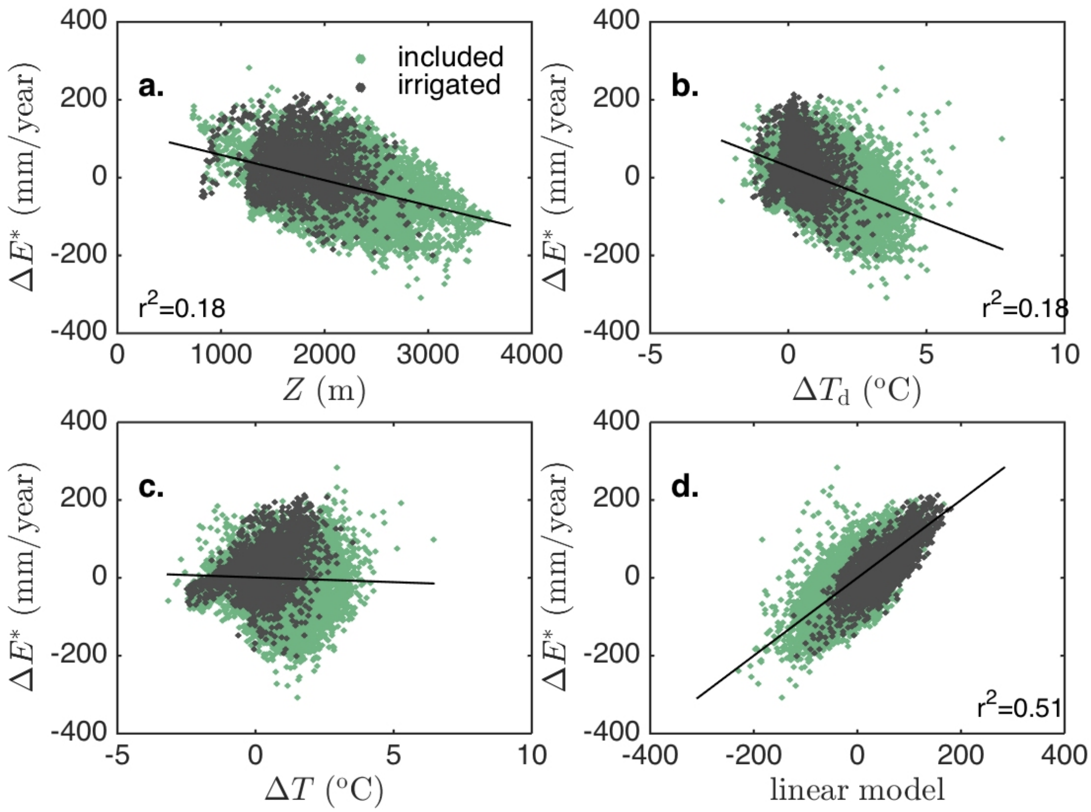

Fig. 8. Linear dependencies of the difference in E with wind and solar effects removed. On the ordinate of each panel, ΔE^{*} denotes ΔE with the effects of ΔV and ΔS linearly removed [i.e., the residuals from the model given by equation (4) shown in Fig. 6d]. On the abscissas are (a) Z indicating elevation in meters, (b) ΔT_d from Fig. 4i, (c) ΔT from Fig. 4f, and (d) the linear model given by equation (5). Green symbols correspond to included grid points (i.e., locations not indicated as excluded in Fig. 2c), and gray symbols correspond to grid points that contain irrigated agriculture as indicated in Fig. 2b. Black lines indicate least squares linear regressions.

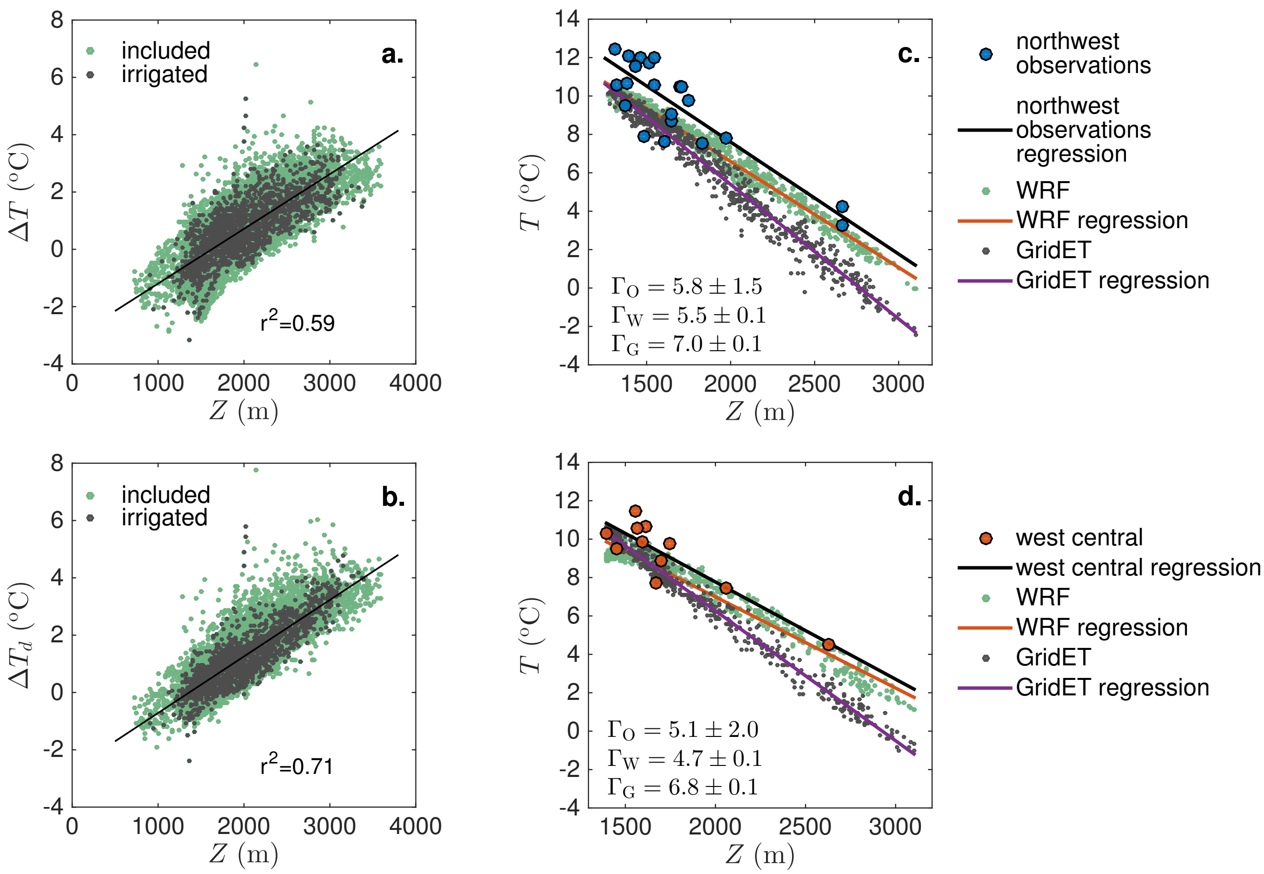

Figure 9. Scatterplots illustrating contrasts in lapse rates. (a) Dependence of ΔT on elevation. Green symbols correspond to included grid points (i.e., locations not indicated as excluded in Fig. 2c), and gray symbols correspond to grid points that contain irrigated agriculture as indicated in Fig. 2b. Black lines indicate least squares linear regressions. (b) Same as (a) but for ΔT_d. (c) Blue circles are observed 1981-2010 fall (September-November) mean temperatures from the NOAA climate normals stations labeled as northwest on the map in Fig. 10, and the black line is a least squares linear regression for these points. The corresponding data for GridET and WRF grid points within the latitude-longitude extent of the northwest climate normal stations are shown with regression lines as indicated in the legend. (d) Same as (c) but for the climate normal stations labeled as west central on the map in Fig. 10.

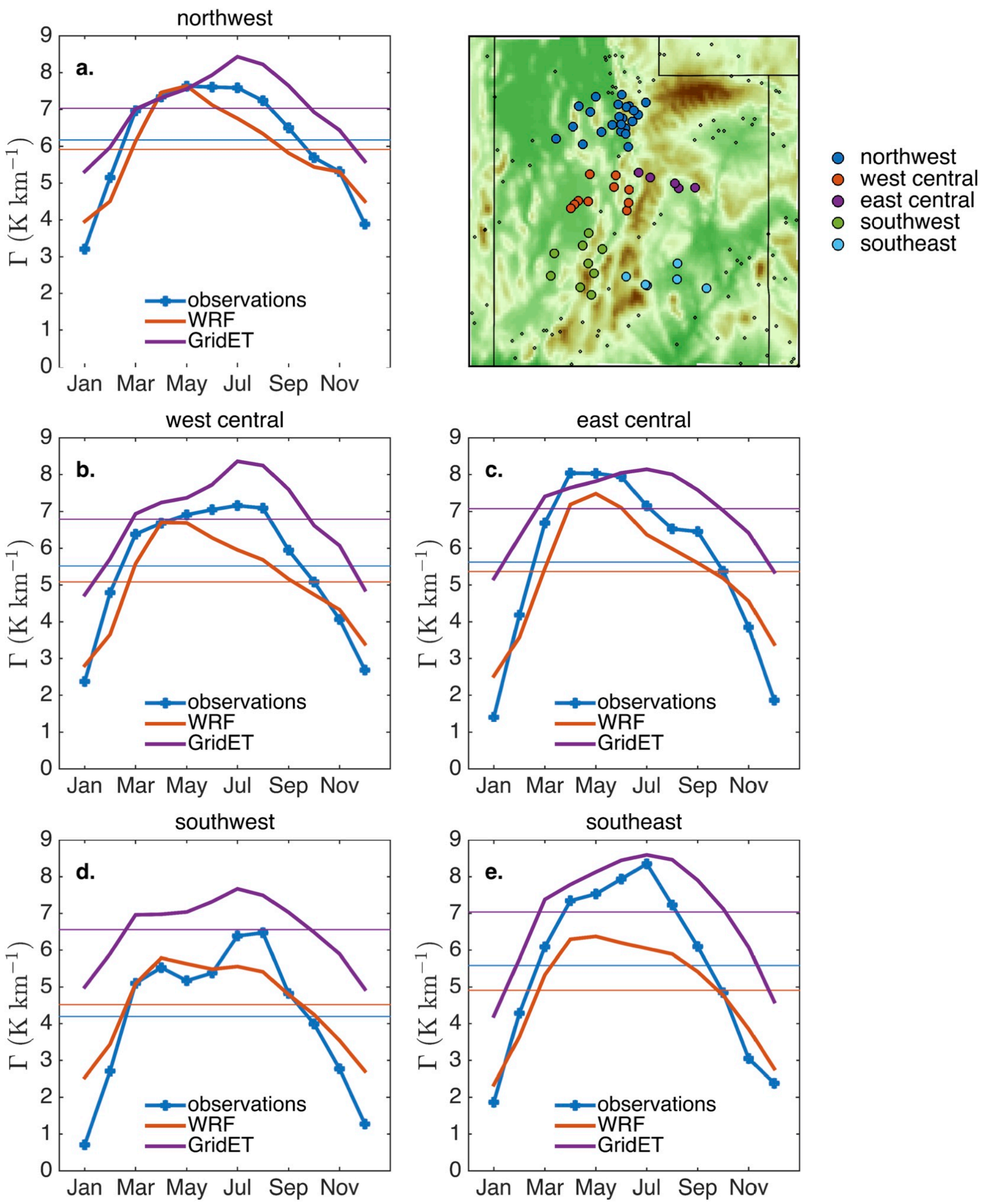

Fig. 10. Lapse rate annual cycles. The map at upper right shows elevation shaded as in Fig. 2a. Large filled circles on the map indicate NOAA climate normals stations used to calculate lapse rates and small circles indicate stations not used. (a) For locations labeled northwest on the map, lapse rate based on observed climate normal (blue curve), based on WRF (orange curve),

and based on GridET (purple curve). (b-e) Same as (a) but for the locations on the map indicated by the title above each panel.

References

Allen, R. et al., 2005. The ASCE standardized reference evapotranspiration equation. American Society of Civil Engineers Environmental and Water Resource Institute (ASCE-EWRI). 59 pp.

Allen, R.G., Pereira, L.S., Howell, T.A., Jensen, M.E., 2011. Evapotranspiration information reporting: I. Factors governing measurement accuracy. Agricultural Water Management, 98(6): 899-920.

Allen, R.G., Pereira, L.S., Raes, D., Smith, M., 1998. FAO Irrigation and drainage paper No. 56. Rome: Food and Agriculture Organization of the United Nations: 26-40.

Allen, R.G., Tasumi, M., Trezza, R., 2007. Satellite-based energy balance for mapping evapotranspiration with internalized calibration (METRIC)—Model. Journal of Irrigation and Drainage Engineering, 133(4): 380-394.

Allen, R.G., Trezza, R., Tasumi, M., 2006. Analytical integrated functions for daily solar radiation on slopes. Agricultural and Forest Meteorology, 139(1–2): 55-73. DOI:http://dx.doi.org/10.1016/j.agrformet.2006.05.012

Arguez, A. et al., 2012. NOAA's 1981–2010 U.S. Climate Normals: An Overview. Bulletin of the American Meteorological Society, 93(11): 1687-1697. DOI:doi:10.1175/BAMS-D-11-00197.1

Berg, A.A., Famiglietti, J.S., Walker, J.P., Houser, P.R., 2003. Impact of bias correction to reanalysis products on simulations of North American soil moisture and hydrological fluxes. Journal of Geophysical Research: Atmospheres, 108(D16). DOI:10.1029/2002JD003334

Bhatt, B.C., Sobolowski, S., King, M.P., 2014. Assessment of downscaled current and future projections of diurnal rainfall patterns for the Himalaya. Journal of Geophysical Research: Atmospheres, 119(22): 12,533-12,545. DOI:10.1002/2014JD022134

Blaney, H.F., Criddle, W.D., 1962. Determining consumptive use and irrigation water requirements. US Department of Agriculture.

Cheng, W.Y.Y., Steenburgh, W.J., 2005. Evaluation of Surface Sensible Weather Forecasts by the WRF and the Eta Models over the Western United States. Weather and Forecasting, 20(5): 812-821. DOI:doi:10.1175/WAF885.1

Coniglio, M.C., Jr., J.C., Marsh, P.T., Kong, F., 2013. Verification of Convection-Allowing WRF Model Forecasts of the Planetary Boundary Layer Using Sounding Observations. Weather and Forecasting, 28(3): 842-862. DOI:10.1175/WAF-D-12-00103.1

Cosgrove, B.A. et al., 2003. Real-time and retrospective forcing in the North American Land Data Assimilation System (NLDAS) project. Journal of Geophysical Research: Atmospheres, 108(D22).

Donohue, R.J., McVicar, T.R., Roderick, M.L., 2010. Assessing the ability of potential evaporation formulations to capture the dynamics in evaporative demand within a changing climate. Journal of Hydrology, 386(1–4): 186-197. DOI:http://dx.doi.org/10.1016/j.jhydrol.2010.03.020

Estévez, J., García-Marín, A., Morábito, J., Cavagnaro, M., 2016. Quality assurance procedures for validating meteorological input variables of reference evapotranspiration in mendoza province (Argentina). Agricultural Water Management, 172: 96-109.

Estévez, J., Gavilán, P., Berengena, J., 2009. Sensitivity analysis of a Penman–Monteith type equation to estimate reference evapotranspiration in southern Spain. Hydrological processes, 23(23): 3342-3353.

Gavilán, P., Estévez, J., Berengena, J., 2008. Comparison of standardized reference evapotranspiration equations in Southern Spain. Journal of Irrigation and Drainage Engineering, 134(1): 1-12.

GridET, 2015. GridET: Gridded Evapotranspiration Estimation. Source Code Repository. <https://github.com/claytonscottlewis/GridET>. (December 22, 2015).

Gutmann, E.D. et al., 2012. A Comparison of Statistical and Dynamical Downscaling of Winter Precipitation over Complex Terrain. J Climate, 25(1): 262-281. DOI:10.1175/2011jcli4109.1

Haagenson, P.L., Dudhia, J., Grell, G.A., Stauffer, D., 1994. he Penn State/NCAR Mesoscale Model (MM5) source code documentation. NCAR Technical Note NCAR/TN-392+STR. DOI:10.5065/D6C24TDV

Hargreaves, G.H., Samani, Z., A., 1985. Reference Crop Evapotranspiration from Temperature. 1(2). DOI:10.13031/2013.26773

Heikkilä, U., Sandvik, A., Sorteberg, A., 2011. Dynamical downscaling of ERA-40 in complex terrain using the WRF regional climate model. Clim Dynam, 37(7): 1551-1564. DOI:10.1007/s00382-010-0928-6

Hill, R., Barker, J., Lewis, C., 2011. Crop and Wetland Consumptive Use and Open Water Surface Evaporation for Utah, Research Report, Utah Agr. Exp. Stn. Res. Report 212 http://uaes.usu.edu/htm/publications/research-reports/research-report-no-212/ (Accessed July 03,2016).

Hobbins, M.T., 2016. The variability of ASCE standardized reference evapotranspiration: A rigorous, CONUS-wide decomposition and attribution. Transactions of the ASABE, 59(2): 561-576. ((doi: 10.13031/trans.59.10975)).

Horvath, K., Koracin, D., Vellore, R., Jiang, J., Belu, R., 2012. Sub-kilometer dynamical downscaling of near-surface winds in complex terrain using WRF and MM5 mesoscale models. Journal of Geophysical Research: Atmospheres, 117(D11): n/a-n/a. DOI:10.1029/2012JD017432

Hupet, F., Vanclooster, M., 2001. Effect of the sampling frequency of meteorological variables on the estimation of the reference evapotranspiration. Journal of Hydrology, 243(3–4): 192-204. DOI:http://dx.doi.org/10.1016/S0022-1694(00)00413-3

Irmak, S., Howell, T.A., Allen, R.G., Payero, J.O., Martin, D.L., 2005. Standardized ASCE Penman-Monteith: impact of sum-of-hourly vs. 24-hour timestep computations at reference weather station sites Transactions of the ASAE 48(3): 1-15.

Irmak, S., Payero, J.O., Martin, D.L., Irmak, A., Howell, T.A., 2006. Sensitivity analyses and sensitivity coefficients of standardized daily ASCE-Penman-Monteith equation. Journal of Irrigation and Drainage Engineering, 132(6): 564-578.

Ishak, A.M., Bray, M., Remesan, R., Han, D., 2010. Estimating reference evapotranspiration using numerical weather modelling. Hydrological Processes, 24(24): 3490-3509. DOI:10.1002/hyp.7770

Janjić, Z.I., 2002. Nonsingular implementation of the Mellor-Yamada level 2.5 scheme in the NCEP Meso model, NCEP Off. Note 437, NCEP, Camp Springs, Md.

Jensen, M.E., Burman, R.D., Allen, R.G., 1990. Evapotranspiration and irrigation water requirements, ASCE, New York.

Jensen, M.E., Haise, H.R., 1963. Estimating evapotranspiration from solar radiation. Proceedings of the American Society of Civil Engineers, Journal of the Irrigation and Drainage Division, 89: 15-41.

Jiménez, P.A., Dudhia, J., 2012. Improving the Representation of Resolved and Unresolved Topographic Effects on Surface Wind in the WRF Model. Journal of Applied Meteorology and Climatology, 51(2): 300-316. DOI:doi:10.1175/JAMC-D-11-084.1

Kalma, J.D., McVicar, T.R., McCabe, M.F., 2008. Estimating Land Surface Evaporation: A Review of Methods Using Remotely Sensed Surface Temperature Data. Surveys in Geophysics, 29(4): 421-469. DOI:10.1007/s10712-008-9037-z

Lawrence, M.G., 2005. The Relationship between Relative Humidity and the Dewpoint Temperature in Moist Air: A Simple Conversion and Applications. Bulletin of the American Meteorological Society, 86(2): 225-233. DOI:doi:10.1175/BAMS-86-2-225

Lewis, C.S., Allen, N.L., 2016. Potential Crop Evapotranspiration and Surface Evaporation Estimates via a Gridded Weather Forcing Dataset. Journal of Hydrology. DOI:http://dx.doi.org/10.1016/j.jhydrol.2016.11.055

Lewis, C.S., Geli, H.M., Neale, C.M., 2014. Comparison of the NLDAS Weather Forcing Model to Agrometeorological Measurements in the western United States. Journal of Hydrology, 510: 385-392.

Maupin, M.A. et al., 2014. Estimated use of water in the United States in 2010. 2330-5703, US Geological Survey.

McMahon, T.A., Peel, M.C., Lowe, L., Srikanthan, R., McVicar, T.R., 2013. Estimating actual, potential, reference crop and pan evaporation using standard meteorological data: a pragmatic synthesis. Hydrol. Earth Syst. Sci., 17(4): 1331-1363. DOI:10.5194/hess-17-1331-2013

McVicar, T.R. et al., 2012. Global review and synthesis of trends in observed terrestrial near-surface wind speeds: Implications for evaporation. Journal of Hydrology, 416–417: 182-205. DOI:http://dx.doi.org/10.1016/j.jhydrol.2011.10.024

McVicar, T.R. et al., 2007. Spatially distributing monthly reference evapotranspiration and pan evaporation considering topographic influences. Journal of Hydrology, 338(3–4): 196-220. DOI:http://dx.doi.org/10.1016/j.jhydrol.2007.02.018

Mesinger, F., DiMego, G., Kalnay, E., Mitchell, K., 2006. North American regional reanalysis. Bulletin of the American Meteorological Society, 87(3): 343.

Meyer, J.D.D., Jin, J., 2016. The response of future projections of the North American monsoon when combining dynamical downscaling and bias correction of CCSM4 output. Clim Dynam: 1-15. DOI:10.1007/s00382-016-3352-8

Minder, J.R., Mote, P.W., Lundquist, J.D., 2010. Surface temperature lapse rates over complex terrain: Lessons from the Cascade Mountains. Journal of Geophysical Research: Atmospheres, 115(D14): n/a-n/a. DOI:10.1029/2009JD013493

Mitchell, K.E. et al., 2004. The multi-institution North American Land Data Assimilation System (NLDAS): Utilizing multiple GCIP products and partners in a continental distributed hydrological modeling system. Journal of Geophysical Research: Atmospheres, 109(D7).

Monteith, J., 1965. Evaporation and environment. The state and movement of water in living organisms. Symposium of the society of experimental biology, Vol. 19 (pp. 205-234). Cambridge: Cambridge University Press.

Norris, J., Carvalho, L.M.V., Jones, C., Cannon, F., 2015. WRF simulations of two extreme snowfall events associated with contrasting extratropical cyclones over the western and central Himalaya. Journal of Geophysical Research: Atmospheres, 120(8): 3114-3138. DOI:10.1002/2014JD022592

Rasmussen, R. et al., 2011. High-Resolution Coupled Climate Runoff Simulations of Seasonal Snowfall over Colorado: A Process Study of Current and Warmer Climate. J Climate, 24(12): 3015-3048. DOI:10.1175/2010jcli3985.1

Roderick, M.L., Rotstayn, L.D., Farquhar, G.D., Hobbins, M.T., 2007. On the attribution of changing pan evaporation. Geophys Res Lett, 34(17): n/a-n/a. DOI:10.1029/2007GL031166

Ruiz-Arias, J.A., Arbizu-Barrena, C., Santos-Alamillos, F.J., Tovar-Pescador, J., Pozo-Vázquez, D., 2016. Assessing the Surface Solar Radiation Budget in the WRF Model: A Spatiotemporal Analysis of the Bias and Its Causes. Monthly Weather Review, 144(2): 703-711. DOI:doi:10.1175/MWR-D-15-0262.1

Saha, S. et al., 2010. The NCEP Climate Forecast System Reanalysis. Bulletin of the American Meteorological Society, 91(8): 1015-1057. DOI:10.1175/2010BAMS3001.1

Scalzitti, J., Strong, C., Kochanski, A.K., 2016. A 26 year high-resolution dynamical downscaling over the Wasatch Mountains: Synoptic effects on winter precipitation performance. Journal of Geophysical Research(121): 3224–3240. DOI:10.1002/2015JD024497

Shimada, S., Ohsawa, T., Chikaoka, S., Kozai, K., 2011. Accuracy of the Wind Speed Profile in the Lower PBL as Simulated by the WRF Model. SOLA, 7: 109-112. DOI:10.2151/sola.2011-028

Skamarock, W.C. et al., 2005. A description of the advanced research WRF version 2, DTIC Document.

Tabari, H., Talaee, P.H., 2014. Sensitivity of evapotranspiration to climatic change in different climates. Global and Planetary Change, 115: 16-23.

Tadesse, T., Senay, G.B., Berhan, G., Regassa, T., Beyene, S., 2015. Evaluating a satellite-based seasonal evapotranspiration product and identifying its relationship with other satellite-derived products and crop yield: A case study for Ethiopia. International Journal of Applied Earth Observation and Geoinformation, 40: 39-54.

Thornthwaite, C.W., 1948. An approach toward a rational classification of climate. Geographical review, 38(1): 55-94.

Thornton, P. et al., 2012. Daymet: Daily surface weather on a 1 km grid for North America, 1980-2011. Oak Ridge National Laboratory Distributed Active Archive Center, Oak Ridge, Tennessee, USA. daymet. ornl. gov/[Verified 14 February 2013]. doi, 10.

USDA, 2014. Farm and Ranch Irrigation Survey (2013), Volume 3 • Special Studies • Part 1, AC-12-SS-1 (Table 26). Issued November 2014 United States Department of Agriculture. Tom Vilsack, Secretary; National Agricultural Statistics Service, Joseph T. Reilly, Administrator.

.

Utah Department of Natural Resources, 2010. 2009 Residential Water Use: Survey Results and Analysis of Residential Water Use for Seventeen Communities in Utah, Utah Department of Natural Resources, Division of Water Resources, November 3, 2010.

Valipour, M., 2015. Importance of solar radiation, temperature, relative humidity, and wind speed for calculation of reference evapotranspiration. Archives of Agronomy and Soil Science, 61(2): 239-255.

Vicente-Serrano, S.M. et al., 2014. Sensitivity of reference evapotranspiration to changes in meteorological parameters in Spain (1961–2011). Water Resources Research, 50(11): 8458-8480.

Wang, W. et al., 2013. Changes in reference evapotranspiration across the Tibetan Plateau: Observations and future projections based on statistical downscaling. Journal of Geophysical Research: Atmospheres, 118(10): 4049-4068. DOI:10.1002/jgrd.50393

Xing, W. et al., 2014. Changes of reference evapotranspiration in the Haihe River Basin: Present observations and future projection from climatic variables through multi-model ensemble. Global and Planetary Change, 115: 1-15.

Zheng, C., Wang, Q., 2015. Spatiotemporal pattern of the global sensitivity of the reference evapotranspiration to climatic variables in recent five decades over China. Stochastic Environmental Research and Risk Assessment, 29(8): 1937-1947.